Analysis of Temperature-Field Error of Computational Fluid Dynamics (CFD) in a New Type of Cigar-Curing Shed

Yu Zhao[1], Xinjie Chen[2], Huan Xiang[3], Tong Li[2], Yuhang Zou[3], Jun Wang[3], Yong Chen[3], Mengran Hu[2], Lei Liu[2,*]

[1]Sichuan Institute of Tobacco Science, Chengdu 610000, China
[2]College of Agriculture, Sichuan Agricultural University, Chengdu 611130, China
[3]Sichuan Tobacco Corporation Deyang Branch, Deyang 618400, China

Abstract: Computational fluid dynamics (CFD) offers a powerful tool for simulating the temperature field within an object and it is widely being used in studies related to tobacco curing. However, there remains a discrepancy between the simulated temperature values and the actual monitoring data. To quantitatively understand temperature simulation errors for a CFD model of a novel cigar-curing shed, the temperature within the cigar-curing area was simulated and errors were calculated. This model produced a relative error between −5% and 4%. The upper monitoring surface of the cigar-curing rack exhibited insignificant errors between 0:00–9:00 and 18:00–24:00 (maximum at 10:00–17:00). The distribution area was relatively disordered, and the negative-error area increased sharply. Furthermore, the simulation performance for the upper monitoring surface was superior to that for the lower surface, particularly at night. The worst results were realized in the lower monitoring surface at 11:00–18:00. The ambient temperature influences the temperature uniformity inside the shed, and a greater surface temperature dispersion led to larger simulation errors. CFD modeling errors are mainly responsible for these differences and offer a primary optimization direction. These errors can be reduced by using correction values. This study offers valuable insights for improving the effectiveness of CFD simulations of drying temperatures, thereby achieving a comprehensive and accurate understanding of the novel drying shed's performance.

Keywords: Cigar; Curing Shed; Curing Temperature; CFD Simulation; Error

DOI: 10.57237/j.jaf.2024.03.002

1 Introduction

Cigars are a special type of air-cured tobacco product [1] that require careful attention to temperature during the curing process. [2, 3] The quality of the cigar leaves is significantly influenced by the performance of the curing shed. [4, 5] In Shifang, Sichuan—a major hub for producing cigar leaves in China—traditional tobacco curing sheds are no longer sufficient for meeting the demands for high-quality cigars. [6] Moreover, there is a scarcity of research focusing on the optimization of cigar-curing facilities. To address this, the Sichuan Tobacco Science Research Institute has developed a new type of cigar-curing shed designed to improve the temperature stability and buffering ability dur-

Funding: China Tobacco Corporation Sichuan Provincial Company regarding research on the Development of High-Quality Cigar Core Curing Facilities and Supporting Modulation Techniques for the Science and Technology Project (Sichuan Tobacco Science, 2021, SCYC202123).

*Corresponding author: Lei Liu, srars@sicau.edu.cn

Received: 30 May 2024; Accepted: 16 July 2024; Published Online: 18 July 2024

ing the curing period. However, the actual performance of this new shed still requires thorough investigation.

Computational fluid dynamics (CFD) offers a powerful tool for simulating the temperature field within an object, enabling three-dimensional quantitative analysis. [7] It is widely being used in studies related to temperature control in dense tobacco curing houses and greenhouses. [8, 9] This analysis method helps to comprehensively understand the temperature status and spatial distribution patterns within the curing shed, thereby aiding in its performance evaluation and subsequent improvements. Despite its potential, there remains a discrepancy between the simulated temperature values calculated using CFD simulation and the actual monitoring data within the curing shed. High-quality temperature simulations are conducive to recognizing the temperature distribution within the cigar-curing shed and improving the authenticity of the simulation data. To date, there have been no systematic studies examining the errors associated with CFD simulations in cigar-curing sheds.

In this study, we collected real-time temperature data from a new type of cigar-curing shed in the Shifang Tobacco District of Sichuan Province. Using CFD technology, we simulated and modeled the temperature field within the shed and calculated the data error at each monitoring site. Our objective was to provide an accurate and comprehensive description of temperature variations inside the curing shed. By analyzing the error patterns in CFD simulations, we aim to refine the simulated temperature values, thereby improving the accuracy and effectiveness of these simulations.

2 Materials and Methods

2.1 Materials

The test was conducted at the High-quality Cigar Core Curing Experimental Base located in Nanquan Town, Shifang City, within Deyang City, Sichuan Province. The area features flat terrain and lacks any unusual heat sources. During the testing period, the prevailing wind direction was predominantly from the northeast and northwest.

The new type of curing shed is oriented along a north-south axis and uses PEP dual-color film—black on the inside and white on the outside—for shading. The structure is built with steel–plastic composite pipe fittings and measures 20 m in length, 6.0 m in width, and 4.0 m in height (Figure 1). It features adjustable roller blinds (20 m long × 1.5 m high) on both longitudinal sides and open gates (3.0 m wide × 2.0 m high) at the north and south ends for ventilation and dehumidification. Internally, the cigar rack spans 18 m in length, 5.2 m in width, and 2.0 m in height, comprising two layers. The top layer of the rack is 2.0 m above the ground, [10] while the lower layer is 1.2 m above the ground.

The cigar variety tested is Dexue 3. The cultivation, harvesting, weaving, and hanging of the tobacco leaves strictly followed local production technical specifications. Leaves were dried using the traditional hanging method, secured by ropes. Temperature data were collected using Benetech GM1365 temperature loggers from Shenzhen Jumaoyuan Technology Co., Ltd.

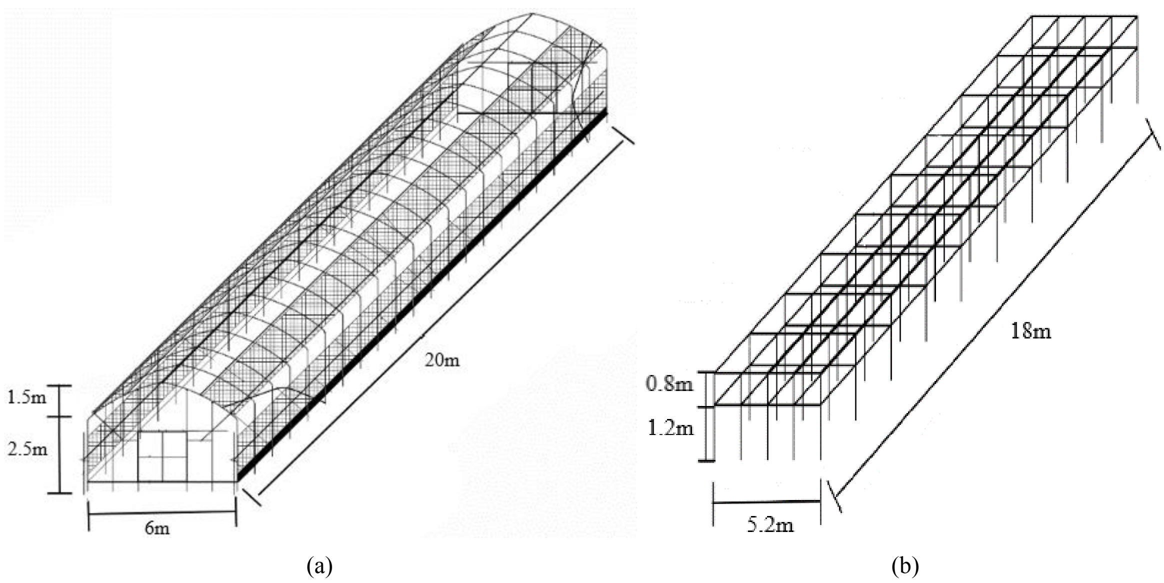

Figure 1 New tobacco air-curing shed (left) and tobacco air-curing rack in shed (right)

2.2 Methods

2.2.1 Distribution of Temperature Monitoring Sites

Data collection occurred from June to July, 2021, with readings taken every 10 min. The layout of the temperature logger inside the cigar rack's space is illustrated in Figure 2. Loggers were arranged in groups every 4.5 m longitudinally (eight loggers in each group), with two groups placed 2.25 m from the north and south boundaries of the cigar rack. They were uniformly distributed across the XOY cross-section. In each group, four loggers were positioned 1.0 m above the ground on the lower layer, and the other four were at 1.8 m above the ground on the upper layer, in the YOZ section. In total, there were 32 temperature loggers deployed within the cigar-curing area.

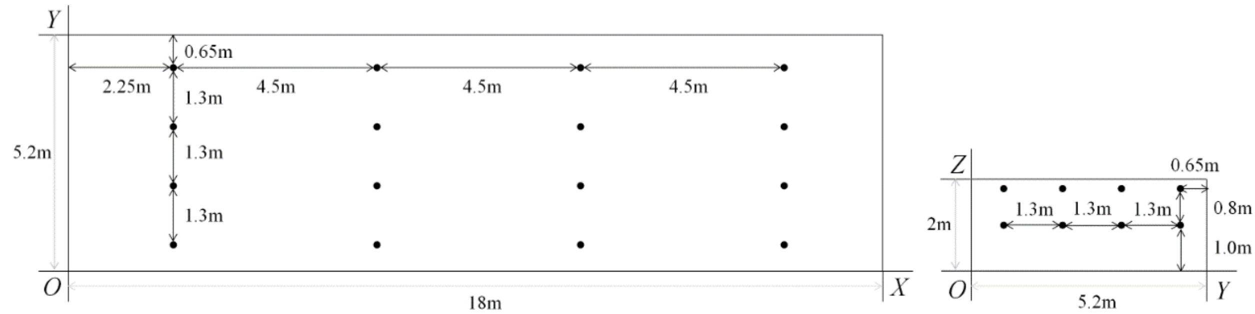

Figure 2 Layout design of temperature recording probes in two-story smoke rack air-curing shed

2.2.2 Physical Model Parameter Setting

To accurately replicate the actual structure of the new curing shed, a 1:1 physical model was created using SolidWorks software. The model featured 32,029 grids, meeting the simulation quality requirements. The flow simulation plugin and the standard *k-ε* turbulence model were employed to perform temperature numerical simulations. [11] Both internal and external heat exchanges occurred via thermal radiation and convection. The fluid within the shed was treated as a low-speed, incompressible fluid at ambient temperature, consistent with the Boussinesq hypothesis. [12] The gas movement process in the shed follows three governing equations: conservation of mass, momentum, and energy. The general form of these equations is as follows [13]:

$$\frac{\partial(\rho\varphi)}{\partial t} + div(pu\varphi) = div(\Gamma\, grad\, \varphi) + S. \quad (1)$$

Here, φ denotes any variable (temperature, density, momentum, etc.), Γ represents the generalized diffusion coefficient, u denotes the velocity vector (m/s), ρ denotes density (kg/m^3), and t represents time (s).

The material properties, thickness, and convection coefficients were specified for the shed's wall film. During the simulation, the side with higher opening temperatures was set as the velocity inlet boundary (v = 0.5 m/s), while all other openings were treated as pressure outlet boundaries (at standard atmospheric pressure). Temperature parameters inside and outside the shed were based on actual measurements and local weather data. The space within the cigar rack was defined as a porous medium with isotropic permeability. The main evaluation index for this porous medium was its porosity, calculated as follows [9]:

$$r = 1 - \frac{\rho_1}{\rho_2}, \quad (2)$$

where ρ_1 denotes the loading density, and ρ_2 denotes the apparent density.

The physical properties of the materials used in the curing are shown in Table 1. The above settings served as the basis to simulate the CFD temperature data.

Table 1 Value table of material properties

Materials	**Density/kg·m^{-3}**	**Specific heat/J·(kg·K)$^{-1}$**	**Heat conductivity coefficient/W·(m·K)$^{-1}$**
Air	1.204	1,007	0.025
PEP film	940	1,380	0.15
Cigar leaf	1,600	3,800	0.086

2.2.3 Drawing of Contour Map of CFD Simulation Error in Curing Shed

The CFD software was utilized to simulate temperature values at each point within the curing shed over various time intervals. These simulated temperatures were then compared with the readings from temperature loggers, considered to be the actual values. The absolute and relative errors were expressed as follows:

$$E_a = x - T,$$

$$E_r = E_a/T \times 100\%. \quad (3)$$

Here, E_a denotes the absolute error, E_r represents the relative error, x represents the simulated temperature value, and T is the value of the monitoring temperature.

This study employed Origin software to generate contour maps for analyzing simulation errors. A rectangular coordinate system was established on both the upper and lower layers of the cigar rack where the monitoring sites were located. The contour maps were plotted based on the X, Y, and E_r (Z) coordinates for each site. To achieve a smooth visual representation, the contour map was set with a total growth factor of 1,000 points and a smoothing parameter of 0.001. Since the boundary of the cigar rack is adjacent to the opening boundary of the curing shed and the error there is approximately 0, the Z-value for each boundary point was set to default at 0.

3 Results and Analysis

3.1 Visualization of Relative Error in Temperature Simulation of the Upper Cigar Rack

Figure 3 depicts the relative error (E_r) in the CFD temperature simulation across the horizontal plane of the upper cigar rack. Over the course of the day, the E_r values range from −5% to 4%. From 0:00 to 9:00 and from 18:00 PM to 24:00, the simulated temperatures closely match the actual measurements and are uniformly distributed across the horizontal space. During these times, only a few areas exhibit warm-tone blocks, indicating a slight positive error (E_r>0). Conversely, between 10:00 and 17:00, the Er values are higher and the distribution of color blocks on the contour map becomes more chaotic. Cold-tone blocks (E_r<0) and warm-tone blocks (E_r>0) intersect, with the areas showing negative errors (Er<0) increasing sharply during periods of high external temperatures. At other times, the contour map is primarily characterized by mid-tone blocks, with warm-tone blocks appearing in small quantities.

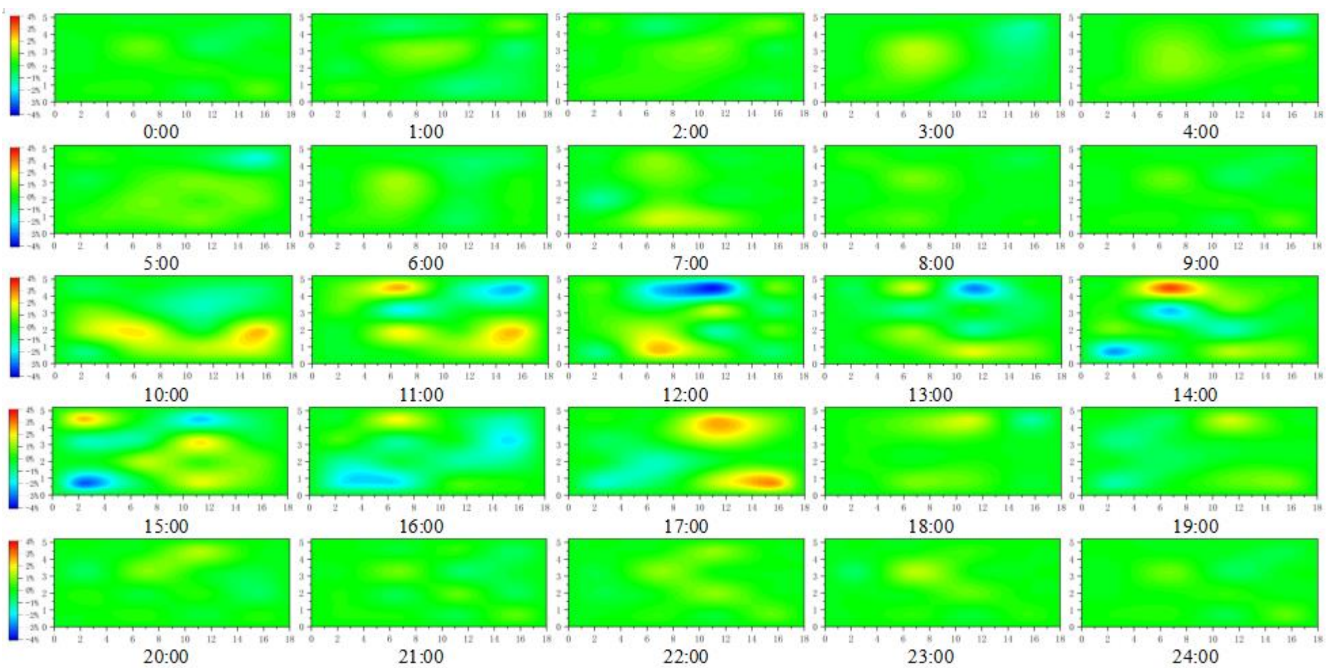

Figure 3 Contour map of simulated temperature error in upper surface at each time points

3.2 E_r Quantitative Analysis of Horizontal Surface

To conduct a quantitative analysis of horizontal temperature error (E_r), we partitioned the E_r values on the horizontal surfaces of both the upper and lower cigar racks at different times, as illustrated in Figure 3. A gradient of 1% was used to calculate the percentage area that each error gradient occupies. As shown in Figure 4, between 0:00 and 9:00, E_r values were largely confined between −1% and 1%, occupying over 90% of the total area, indicating low variability. However, from 10:00 to 17:00, there was a notable increase in E_r values, peaking at −3.40% at 12:00. During this period, the area with E_r<0 also increased and reached its maximum coverage of approximately 70.85% at 16:00. After 18:00, E_r values continued to decrease and returned to between −1% and 1% range. Overall, the upper monitoring surface in the cigar-curing area exhibited a daily temperature error range of −4% to 3%, indicative of satisfactory simulation accuracy.

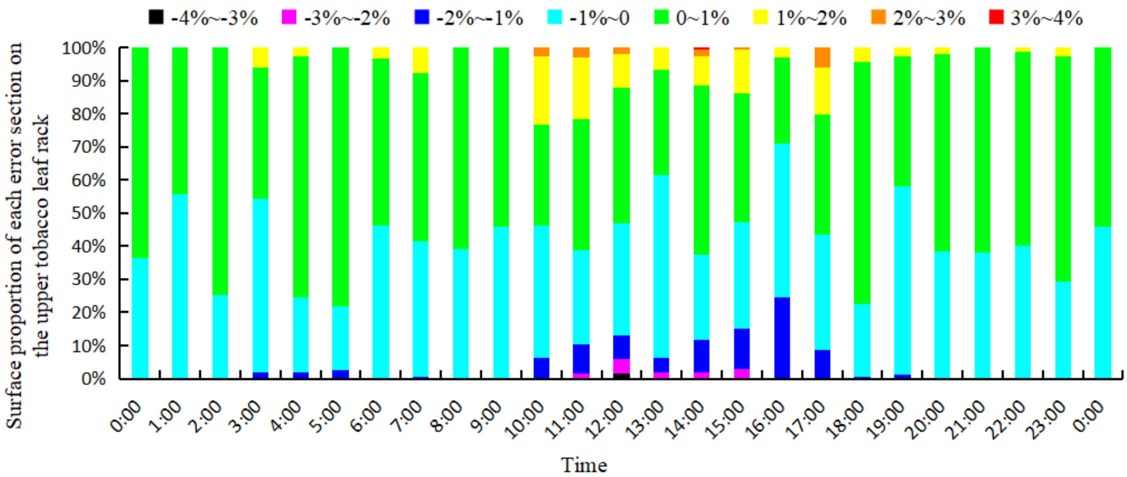

Figure 4 Surface ration of each error gradient in upper monitoring surface at different time points

Figure 5 shows the area ratio of each error gradient on the plane where the lower monitoring sites in the cigar-curing area are located. Contrary to the upper monitoring surface, for the lower monitoring sites, the gradient area with E_r>0 was significantly greater than the area with E_r<0 between 0:00 and 9:00, peaking at 78.27% at 5:00. Starting at 10:00, the area with E_r<0 expanded considerably, achieving full coverage (100%) at 16:00. At 12:00, an error range between −5% and −4% appeared, reaching a maximum error of −4.54%, pointing to reduced simulation accuracy. After 19:00, the E_r values on the lower monitoring surface gradually decreased, and the distribution of the area ratios for each gradient became similar to those on the upper monitoring surface.

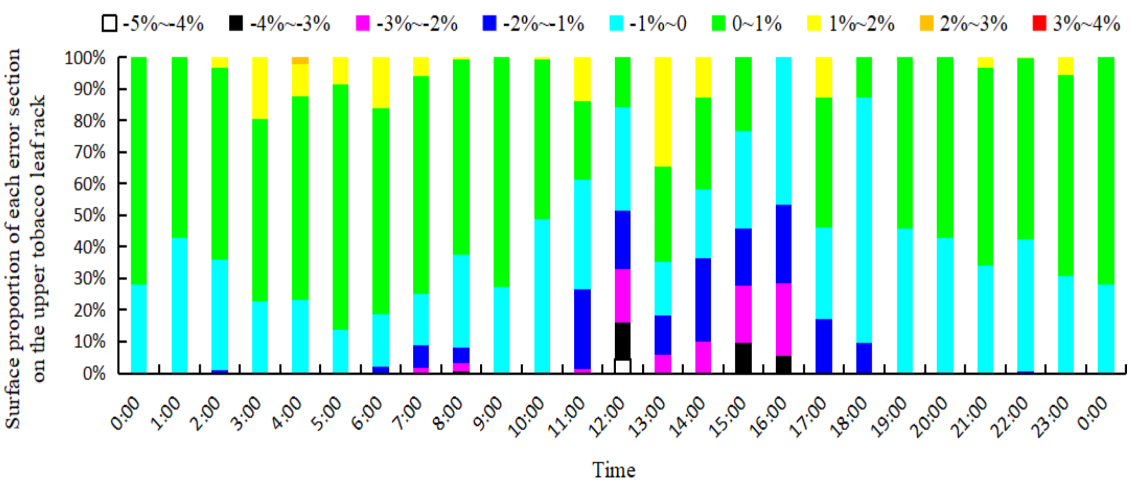

Figure 5 Surface ratio of each error gradient in the lower monitoring surface at different time points

3.3 Analysis of Error Distribution Uniformity in Monitoring Surface

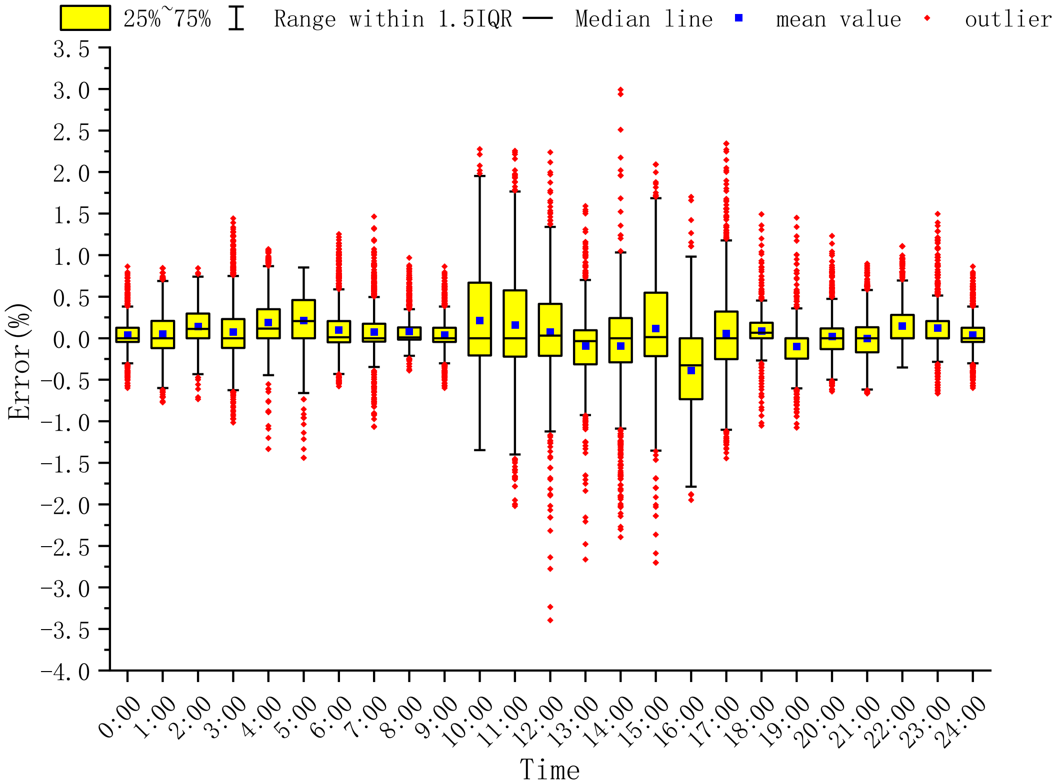

Figure 6 Box plot of distribution of error in upper monitoring surface

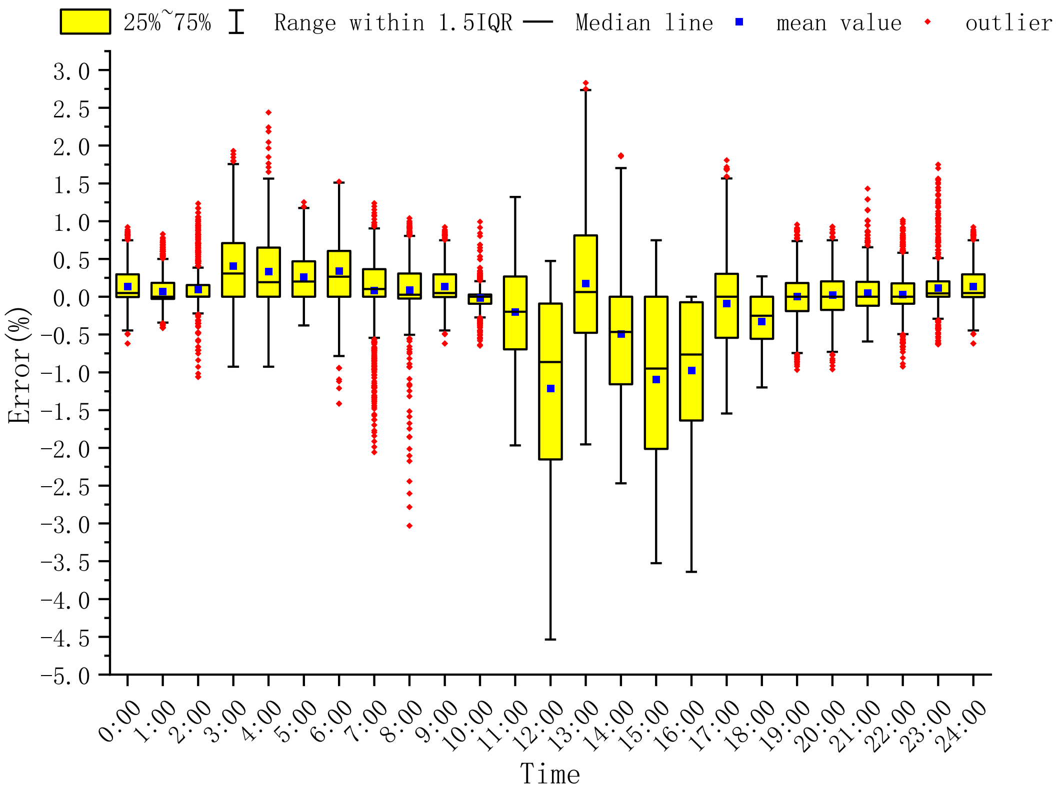

Figure 7 Box plot of distribution of error in lower monitoring surface

Data extracted from the E_r contour map, which included 30×30 simulated error point values, was used to create a box plot to analyze the distribution uniformity of error values (E_r) across different time points on the monitoring surface. Figure 6 presents the box plot for the upper monitoring surface. Across various time periods, both the median and mean values of E_r generally remained around 0, displaying minor shifts between 5:00 and 16:00, thus indicating good symmetry. The range of E_r values was notably broader between 10:00 and 17:00, particularly within the 25% to 75% quartile range. The dispersion was most uneven at 10:00. At each time point, there were outliers that exceeded 1.5 times the interquartile range (IQR), with the maximum span reaching 5.63% at 12:00.

Figure 7 shows a significantly different distribution for the lower monitoring surface. The symmetry of the E_r box plot was relatively poor, spanning from 3:00 to 18:00. At 12:00, 15:00, and 16:00, the median and mean values settled at approximately −1%, deviating noticeably from the zero-error scale between 3:00 to 6:00 and 13:00 to 14:00. In terms of E_r range, between 3:00 to 6:00 and 11:00 to 17:00 the distribution was notably dispersed within the 25% to 75% quartile range. The widest interval and value spans occurred at 12:00, measuring 2.06% and 5.00%, respectively, marking it as the time with the most uneven distribution.

3.4 Analysis of Correlation Between Temperature Simulation Error of Monitoring Surface and Various Temperature Indicators Inside and Outside Curing Shed

To deepen our understanding on the correlation between simulated temperature error (E_r) on each monitoring surface with actual temperatures inside and outside the shed, we examined several variables. These included the external atmospheric temperature at each time point (T), the temperature difference between adjacent points (ΔT), the true temperature dispersion on each monitoring surface (the upper surface: σ_U, the lower surface: σ_L), the overall true temperature dispersion in the cigar-curing area (σ_A), and the average absolute simulated error values on each surface ($\bar{E}_r$). These relationships are illustrated in the subsequent heat map.

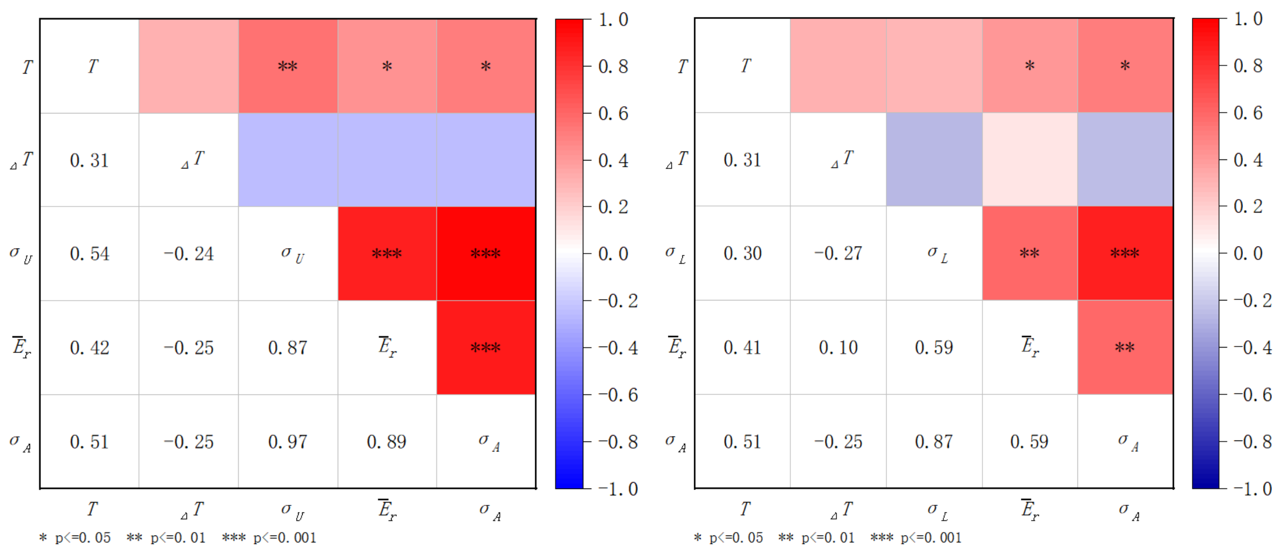

(a) (b)

Figure 8 Heat map of correlation analysis between error of upper (left) and lower (right) surface and various temperature value of inside and outside air-curing shed

As illustrated in Figure 8 (left), T and σ_U had very significant correlation (p<0.01) and was significant between σ_A(p<0.05), with correlation coefficients of 0.54 and 0.51, respectively. This indicated that the external temperature has a certain impact on the temperature uniformity of both the upper monitoring surface and entire curing shed. However, the temperature difference between adjacent points (ΔT) showed no significant correlation with other indicators, implying that fluctuations in external temperature have no significant impact on the uniformity of temperature and E_r. Notably, the correlation coefficients between $\bar{E}_r$ of the upper monitoring surface and σ_U, $\bar{E}_r$ and σ_A reached 0.87 and 0.89, respectively, both of which were extremely significant (p<0.001). This reveals that greater dispersion and unevenness in actual temperatures at monitored sites correspond to higher simulated errors.

The right side of Figure 8 shows the relationship between the E_r on the lower monitoring surface and various temperature indicators inside and outside the curing shed. Here, the correlation between T and σ_L was not significant (p>0.05). Moreover, the correlation coefficient decreased by 0.24 compared to σ_U, suggesting that the external temperature had a minimal effect on the temperature uniformity of the lower monitoring surface. Similar to observations for the upper layer, changes in ΔT had no significant impact on other temperature indicators. However, the correlation between $\bar{E}_r$, σ_L, and σ_A was found to be significant (p<0.01), with a correlation coefficient of 0.59. This indicates that the temperature dispersion monitored in the cigar-curing area does have a certain level of influence on the E_r of the lower monitoring surface, showing a positive correlation.

4 Discussion

Obtaining the overall temperature dynamics of cigar leaves during the curing process is crucial for tracking changes in their quality. This study employed CFD simulation software to simulate the temperature conditions inside a cigar-curing shed. While the results were promising, minor inaccuracies persisted. To address this, we used Origin software to generate error contour maps for the monitoring sites located both above and below the curing shed. These maps offer a quantitative analysis of temperature differences caused by the CFD simulations and serve as a foundation for future refinements in simulating the shed's temperature environment more accurately.

Our analysis explored the correlation between the E_r of simulated temperature and various temperature indicators both inside and outside the curing shed. We found that external temperature impacts the uniformity of the monitored surface temperatures inside the shed. Specifically, greater temperature dispersion across a single monitoring surface correlates with increased simulation error. The errors in temperature simulation of shed are mainly caused by three aspects: modeling errors, which arise from control equations, boundary conditions, and physical parameters; discretization errors, attributed to the discretization format and grid density distribution; and calculation errors, resulting from rounding and iterative processes in computational methodology. [14, 15] Physical indicators such as temperature, humidity, airflow, and air pressure are in constant flux within the curing shed, as indicated by prior studies. [16] Additional variables such as uneven density in the drying area, [17, 18] thermal conductivity, [19] and morphological changes [20] in the cigar leaves introduce further uncertainties into the simulation. Typically, CFD simulations use specific control equations, boundary conditions, and physical parameters to represent conditions at all times. [8, 11] However, our correlation analysis results indicated that these physical parameters fluctuate across different horizontal positions on the same monitoring surface. Moreover, cigar leaves at different locations respond variably to environmental temperatures, leading to discrepancies between simulated and actual temperatures. Therefore, the primary avenues for reducing CFD simulation errors include optimizing the physical parameters related to both the curing shed and the cigar leaves, as well as adopting control equations that more accurately reflect the dynamic changes occurring during the drying period [9, 21].

By analyzing the error contour maps, error gradient area proportion maps, and box plots, we can draw several conclusions. The upper monitoring surface displays lower simulated temperature errors during periods of low external temperatures, and the ranges of both E_r>0 and E_r<0 are relatively consistent. However, during periods of high external temperatures, the simulated error on the monitoring surface increases, the span of error values increases, and distribution uniformity deteriorates. In particular, the area range occupied by E_r<0 increases sharply during this stage. The error variation pattern on the lower monitoring surface largely mirrors that of the upper surface, particularly between 11:00 and 18:00. During this period, the error and dispersion increase significantly. The lower monitoring surface is primarily characterized by E_r<0, indicating a decline in simulation quality compared to the upper surface. This discrepancy might stem from the upper surface's closer proximity to the upper air layer, where CFD analysis of airflow changes is more accurate for the complex interiors of cured cigar bodies. Nighttime simulations are generally more accurate than daytime ones, possibly due to the more complex heat transfer mechanisms operating inside the curing shed during the day. [9]

Numerical methods face challenges in accounting for various factors over the simulation period. Paliwal et al. [22] corrected simulated values and reduced errors by identifying independent error sources in CFD validation experiments to improve simulation accuracy. Similarly, Wustenhagen et al. [23] employed different methods to calculate deviations in CFD and provide reliable estimates of simulation errors. Based on these analyses, we can compile correction values for different time periods and positions of the new type of cigar-curing shed. Implementing these corrections will improve overall simulation quality, enabling a more accurate and easily understood representation of temperature distribution within the shed across various time periods. This, in turn, can be applied to actual production activities to enhance the quality of cigar curing.

5 Conclusions

In this study, we developed a temperature simulation model for a new type of cigar-curing shed based on CFD. The model yielded promising results, featuring a low margin of error. For the first time, we used contour maps to visualize the spatial distribution of these errors. Furthermore, we conducted a quantitative analysis of the temporal and spatial distribution patterns of temperature simulation errors in the drying shed. Our findings indicate that the simulation is more accurate for the upper monitoring surface of the shed than for the lower one, and that it performs better at night than during the day. One critical observation is that external temperatures influence the temperature uniformity inside the shed. Specifically, a larger dispersion in measured temperatures within the monitoring area correlates with greater CFD simulation errors. These discrepancies are primarily due to differences in the physical properties between the simulated environment and actual conditions. The study also sheds light on how modeling errors impact temperature simulations, offering valuable insights for future refinements. By understanding these factors, we can formulate simple calibration values tailored for different positions and times. These calibrations will enable us to fine-tune the simulated temperatures, thereby reducing errors and improving the model's overall accuracy.

Author Contributions

Yu Zhao and Xinjie Chen contributed equally to this work. Conceptualization: Yu Zhao and Lei Liu; methodology: Xinjie Chen and Lei Liu; software: Xinjie Chen; validation: Xinjie Chen, Tong Li, Mengran Hu, and Lei Liu; formal analysis: Xinjie Chen; investigation: Yu Zhao, Huan Xiang, Yuhang Zou, and Jun Wang; resources: Yu Zhao; data curation: Xinjie Chen; writing—original draft preparation: Xinjie Chen; writing—review and editing: Lei Lei; visualization: Xinjie Chen; supervision: Yu Zhao and Lei Liu; project administration: Yu Zhao,Huan Xiang, Yuhang Zou, Jun Wang, and Yong Chen; funding acquisition: Yu Zhao. All authors have read and agreed to the published version of the manuscript.

Data Availability Statement

The datasets used and/or analyzed during the current study are available from the corresponding author upon reasonable request.

Conflicts of Interest

The authors declare no conflict of interest.

References

[1] Hu, W. R.; Zhou, Q. W.; Cai, W.; Liu, J.; Li, P.; Hu, D.; Luo, C.; Li, D. Effects of coffee and cocoa as fermentation additives on sensory quality and chemical compositions of cigar tobacco leaves. *Food Sci Technol* 2023, *43*. https://doi.org/10.1590/fst.96122

[2] Jia, J. X.; Zhang, M. J.; Zhao, J. C.; Wang, J.; He, F.; Wang, L. The effects of increasing the dry-bulb temperature during the stem-drying stage on the quality of upper leaves of flue-cured tobacco. *Processes* 2023, *11*(3), 726. https://doi.org/10.3390/pr11030726

[3] Liu, H.; Duan, S.; Luo, H. Design and temperature modeling simulation of the full closed hot air circulation tobacco bulk curing barn. *Symmetry* 2022, *14*(7), 1300. https://doi.org/10.3390/sym14071300

[4] Zhang, Q.; Kong, G. H.; Zhao, G. K.; Liu, J.; Jin, H.; Li, Z.; Zhang, G.; Liu, T. Microbial and enzymatic changes in cigar tobacco leaves during air-curing and fermentation. *Appl Microbiol Biotechnol* 2023, *107*, 5789–5801. https://doi.org/10.1007/s00253-023-12663-5

[5] Gao, L. Studies on dynamic changes of physiological and biochemical indexes and its relationship with quality in burley tobacco 2005.

[6] Yuhang, Z.; Yizhi, T.; Huashu, Z.; et al. Preliminary study on the technology of cigar clothing and cigarette blending. *China Agric Inf* 2015, *01*, 83–84.

[7] Chao, Y.; Jian, Y.; Jinglei, X.; et al. Development achievements and prospects of CFD simulation methods. *Prog Mech* 2011, *41*, 562–589.

[8] Cheng, X.; Li, D.; Shao, L.; Ren, Z. A virtual sensor simulation system of a flower greenhouse coupled with a new temperature microclimate model using three-dimensional CFD. *Comput Electron Agric* 2021, *181*, 105934. https://doi.org/10.1016/j.compag.2020.105934

[9] Bai, Z.; Guo, D.; Li, S.; Hu, Y. Analysis of temperature and humidity field in a new bulk tobacco curing barn based on CFD. *Sensors* 2017, *17*(2), 279. https://doi.org/10.3390/s17020279

[10] Xinjie, C.; Yu, Z.; Huan, X.; et al. Analysis of temperature and humidity field in a new type of cigar tobacco leaf drying shed based on CFD. *Chin J Tob* 2023, *29*, 135–144.

[11] Piscia, D.; Montero, J. I.; Baeza, E.; Bailey, B. J. A CFD greenhouse night-time condensation model. *Biosyst Eng* 2012, *111*(2), 141–154. https://doi.org/10.1016/j.biosystemseng.2011.11.006

[12] Chen, J. L.; Cai, Y. W.; Xu, F.; Hu, H.; Ai, Q. Analysis and optimization of the fan-pad evaporative cooling system for greenhouse based on CFD. *Adv Mech Eng* 2014, 6. https://doi.org/ 10.1155/2014/712740

[13] Thorpe, G. R. The application of computational fluid dynamics codes to simulate heat and moisture transfer in stored grains. *J Stored Prod Res* 2008, *44*(1), 21–31. https://doi.org/10.1016/j.jspr.2007.07.001

[14] Wiser, R. A First Complete Approach to Address Model Error in Computational Turbulent Heat Transfer. Dissertation, Massachusetts Institute of Technology, Cambridge, MA, USA, 2023.

[15] Hu, G. Uncertainty Assessment for CFD Using Error Transport Equation. Dissertation, West Virginia University, Morgantown, WV, USA, 2002.

[16] Xu, K.; Guo, X.; He, J. M.; Yu, B.; Tan, J.; Guo, Y. A study on temperature spatial distribution of a greenhouse under solar load with considering crop transpiration and optical effects. *Energy Convers Manag* 2022, *254*, 115277. https://doi.org/10.1016/j.enconman.2022.115277

[17] Yeo, U.-H.; Lee, S.-Y.; Park, S.-J.; Kim, J.-G.; Choi, Y.-B.; Kim, R.-W.; Shin, J. H.; Lee, I.-B. Rooftop greenhouse: (1) design and validation of a BES model for a plastic-covered greenhouse considering the tomato crop model and natural ventilation characteristics. *Agriculture* 2022, *12*(7), 903. https://doi.org/10.3390/agriculture12070903

[18] Boulard, T.; Roy, J. C.; Pouillard, J. B.; Fatnassi, H.; Grisey, A. Modelling of micrometeorology, canopy transpiration and photosynthesis in a closed greenhouse using computational fluid dynamics. *Biosyst Eng* 2017, *158*, 110–133. https://doi.org/10.1016/j.biosystemseng.2017.04.001

[19] Sun, J.; Chen, Y.; Liu, L.; Zhu, F.; Li, Z.; Yu, L.; Xu, S.; Yue, Y.; Ma, Y.; Li, D. Simultaneous measurement of temperature-dependent thermal conductivity and heat capacity of an individual cured tobacco leaf. *Int J Thermophys* 2021, *42*. https://doi.org/10.1007/s10765-021-02881-2

[20] Zhao, S.; Wu, Z.; Lai, M.; Zhao, M.; Lin, B. Determination of optimum humidity for air-curing of cigar tobacco leaves during the browning period. *Ind Crops Prod* 2022, *183*, 114939. https://doi.org/10.1016/j.indcrop.2022.114939

[21] Li, K.; Xue, W.; Mao, H.; Chen, X.; Jiang, H.; Tan, G. Optimizing the 3D distributed climate inside greenhouses using multi-objective optimization algorithms and computer fluid dynamics. *Energies* 2019, *12*(15), 2873. https://doi.org/10.3390/en12152873

[22] Paliwal, N.; Damiano, R. J.; Varble, N. A.; Tutino, V. M.; Dou, Z.; Siddiqui, A. H.; Meng, H. Methodology for computational fluid dynamic validation for medical use: Application to intracranial aneurysm. *J Biomech. Eng* 2017, *139*(12), 1210041. https://doi.org/10.1115/1.4037792

[23] Wüstenhagen, C.; John, K.; Langner, S.; Brede, M.; Grundmann, S.; Bruschewski, M. CFD validation using in-vitro MRI velocity data - Methods for data matching and CFD error quantification. *Comput Biol Med* 2021, *131*, 104230. https://doi.org/ 10.1016/j.compbiomed.2021.104230